Biomedical Engineering Letters (2024) 14:859–866
https://doi.org/10.1007/s13534-024-00381-4

ORIGINAL ARTICLE

Development of nanogap-rich hybrid gold nanostructures by use of two non-lithographic deposition techniques for a sensitive and reliable SERS biosensor

Hyuck Ju Kwon[1] · Yong Jun Cho[1] · Kyeong Min Yuk[1] · Jonghwan Lee[2] · Seung Ho Choi[3] · Kyung Min Byun[1]

Received: 1 November 2023 / Revised: 24 March 2024 / Accepted: 21 April 2024 / Published online: 29 May 2024

Abstract
Practical application of surface-enhanced Raman spectroscopy (SERS) has suffered from several limitations by heterogeneous distribution of hot-spots, such as high signal fluctuation and the resulting low reliability in detection. Herein, we develop a strategy of more sensitive and reliable SERS platform through designing spatially homogeneous gold nanoparticles (GNPs) on a uniform gold nanoisland (GNI) pattern. The proposed SERS substrate is successfully fabricated by combining two non-lithographic techniques of electron beam evaporation and convective self-assembly. These bottom-up methods allow a simple, cost-effective, and large-area fabrication. Compared to the SERS substrates obtained from two separate nanofabrication methods, Raman spectra measured by the samples with both GNPs and GNIs present a significant increase in the signal intensity as well as a notable improvement in signal fluctuation. The simulated near-field analyses demonstrate the formation of highly amplified plasmon modes within and at the gaps of the GNP-GNI interfaces. Moreover, the suggested SERS sensor is evaluated to detect the glucose concentration, exhibiting that the detection sensitivity is improved by more than 10 times compared to the sample with only GNI patterns and a fairly good spatial reproducibility of 7% is accomplished. It is believed that our suggestion could provide a potential for highly sensitive, low-cost, and reliable SERS biosensing platforms that include many advantages for healthcare devices.

Keywords Hybrid gold nanostructure · Surface-enhanced Raman scattering · Gold nanoislands · Gold nanoparticles · Nanogap · Reliability · Sensitivity

1 Introduction

Raman spectroscopy has been widely utilized in non-invasive and non-destructive detection of molecular-specific vibrations because it can provide distinctive spectral data depending on the target molecules [1]. However, due to its weak scattering intensity, several bothersome signal processing techniques are demanded for accurate identification. In recent years, many researchers have investigated the effect of surface-enhanced Raman spectroscopy (SERS) to amplify the Raman signal via localized surface plasmon resonance (LSPR) phenomenon [2].

While it has been known that the introduction of metallic nanoparticles based on bottom-up fabrication approaches is efficient for the SERS effect [3], this method often suffers from low reproducibility due to the aggregation or non-uniform distribution of gold nanoparticles (GNPs) [4]. In other words, spatial inhomogeneity of LSPR distribution caused by

Hyuck Ju Kwon and Yong Jun Cho are contributed equally to this work.

✉ Seung Ho Choi
seunghochoi@yonsei.ac.kr

✉ Kyung Min Byun
kmbyun@khu.ac.kr

[1] Department of Electronics and Information Convergence Engineering, Kyung Hee University, Yongin 17104, Republic of Korea

[2] School of Engineering, Brown University, Providence, RI 02912, USA

[3] Department of Biomedical Engineering, Yonsei University, 1 Yonseidae-Gil, Wonju, Gangwon-Do 26493, Republic of Korea

non-uniform pattern of GNPs can lead to a large fluctuation in SERS signals.

On the other hand, top-down approaches have been very effective for producing periodic nanostructures in a long range. The most common top-down method involves lithographic patterning techniques using short-wavelength optical sources [5]. A key advantage of the top-down approach is that the parts are both patterned and built in place, so that no chemical assembly step is required. Short-wavelength optical lithography is a relatively mature field because of the high degree of refinement for reaching dimensions below 100 nm [6]. Also, scanning beam techniques such as electron beam or focused ion beam lithography provide the nanostructure size down to about 20 nm. Fairly good resolution and high periodicity of lithographic methods are useful for achieving the reliability in SERS characteristics. However, these top-down processes still have the demerits of expensive and time-consuming lithographic fabrication. Moreover, due to the inherent limitations in controlling the inter-particle gaps, SERS substrates tend to yield relatively lower enhancement and limited sensitivity [7].

In our previous studies, we reported that the highly homogeneous structure of gold nanoislands (GNIs) worked successfully as a sensitive and reliable SERS substrate [8]. The distribution of GNIs was obtained to be quasi-uniform via a simple yet efficient non-lithographic process of gold evaporation on the substrate. Highly uniform pattern of GNIs in a large area allowed a very low standard deviation less than 5% from SERS mapping data. In addition, we demonstrated that surface treatment based on convective self-assembly (CSA) has been beneficial for pattering GNPs in a controllable way [9]. Despite a few practical constraints related to evaporation and convection occurring at a much larger volume than the nanoparticle size, CSA method is advantageous due to its versatility and scalability.

Inspired by this, we intend to attempt a unique design of combining two non-lithographic deposition methods to surmount the limit in the reliability of conventional SERS substrate based on bottom-up methods. More specifically, we propose a novel nanostructured SERS substrate with both GNIs and GNPs, which can provide a synergistic effect of mixing the advantages of high spatial uniformity of GNIs and high signal enhancement of GNPs. Then, we measure and compare the SERS characteristics obtained from 4-ABT experiments among the fabricated samples. Finally, it will be shown that our SERS substrate could be useful for sensitive detection of glucose molecules for diagnosing diabetes.

2 Materials and methods

2.1 Materials

Distilled water (H_2O) and ethyl alcohol (C_2H_5OH) were obtained from Daejung Chemicals & Metals (Siheung, Korea). 4-aminobenzenethiol (4-ABT, C_6H_7NS), 4-mecaptophenyl boronic acid (4-MPBA, $C_6H_7BO_2S$), glucose ($C_6H_{12}O_6$), and cysteamine (C_2H_7NS) were purchased from Sigma-Aldrich (St. Louis, MO, USA). GNPs with an average diameter of 30 nm were purchased from Nanopartz (Loveland, CO, USA).

2.2 Fabrication process of GNIs and GNPs

Fabrication process for realizing the proposed SERS substrate is presented in Fig. 1. A 4-inch silicon wafer was cleaned with an organic solvent in order to remove any organic contaminants. The wafer was rinsed with ethyl alcohol for 5 min and distilled water for 5 min, cleaned again with ethyl alcohol for 5 min, and dried with nitrogen gas for 10 min. Next, a 6-nm thick gold layer was deposited by electron beam evaporation at a deposition rate of 0.2 Å/s. The silicon wafer with uniform GNI patterns was then diced into pieces of 10×10 mm^2 using a dicing machine. The substrate surface was cleaned via sonication in acetone and ethyl alcohol sequentially for 10 min and rinsed with distilled water and ethyl alcohol for 5 min, and dried with nitrogen gas. The substrate was incubated with a 1 mM concentration of cysteamine for a duration of 24 h. Cysteamine was found to bind to the substrate via gold-thiol chemistry, resulting in the hydrophilic modification of the substrate surface [10]. To remove any unbound cysteamine, the substrate was washed with the distilled water for 5 min. Then, GNPs with a concentration of 5 optical density were activated by heating at 40 °C for 1 h. The silicon wafer was immersed into a GNP solution with a depth of 2 mm. At the same time, a syringe pump (KDS-210, KD Scientific, Holliston, USA) was used to draw the GNP solution at a rate of 4.95 μL/h to form a meniscus line on the wafer substrate [11]. Kapton tape was used as a protective layer to avoid the adsorption of GNPs onto the other side of the substrates. GNPs were deposited at the meniscus line region via evaporation, which is associated with evaporation-induced upward convection [12, 13]. Moreover, the attached GNPs were strongly bound and no destruction or damage to the pattern was found during or after the washing, cleaning, and binding processes. The substrate surface was cleaned with an organic solvent in order to remove any organic contaminants.

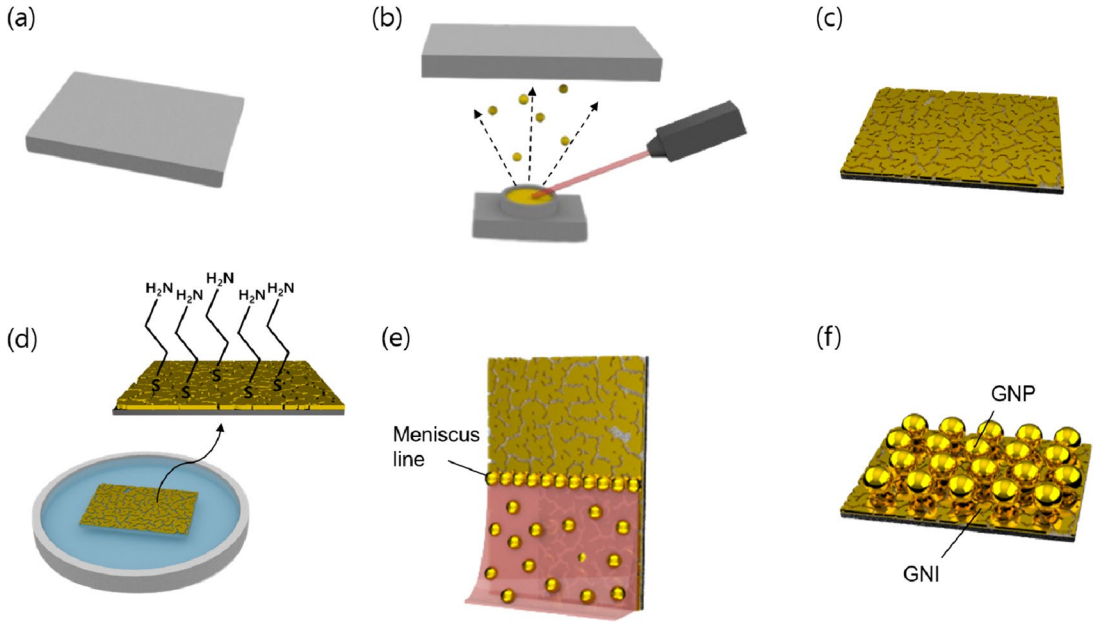

Fig. 1 Fabrication procedure for creating GNIs and GNPs on a silicon wafer substrate. **a** Preparation of a silicon wafer. **b** Gold deposition via electron beam evaporation. **c** Formation of GNIs. **d** Surface modification by use of cysteamine. **e** Convective self-assembly for immobilizing GNPs. **f** Final production of hybrid gold nanostructures with GNPs and GNIs

2.3 SERS experiments

To investigate SERS characteristics of the fabricated samples, Raman signals of 4-ABT were measured. 4-ABT is generally employed as an ideal SERS signaling molecule [14]. It has been known that 4-ABT has a strong SERS activity due to the large Raman cross-section of the benzene ring and the additional chemical enhancement effect [15]. In this study, 4-ABT was used as a target analyte to form well-ordered and stable self-assembled monolayers on SERS-active gold surfaces via strong S–Au bonds. After the SERS substrates were immersed for 15 min in a 1 mM concentrations of 4-ABT solution, the substrates were rinsed with ethyl alcohol and deionized water for 5 min for non-immobilized 4-ABT removal. Raman spectra of 4-ABT were obtained at five different points with an acquisition time of 50 s and a magnification of 100 times. Our experimental setup for Raman spectra measurements was composed of a microscope (BX43, Olympus, Tokyo, Japan), a continuous-wave laser (785 nm, 350 mW, I0785MM0350MF, Innovative Photonic Solutions, Plainsboro Township, NJ, USA), a spectrometer (SR-303i-A, Andor Technology, Belfast, UK) and a low dark current deep-depletion CCD detector (iVac, Andor Technology, Belfast, UK). The diameter of a laser beam spot was approximately 10 μm and the SERS spectrum was obtained within the wavenumber range of 600–1800 cm^{-1}. For the samples with GNPs, the laser beam was placed to illuminate the region of about 30 μm away from the top of meniscus line to avoid a multi-layered GNP pattern, which can highly degrade the linearity characteristics.

2.4 Glucose molecule detection

For glucose detection, 4-MPBA molecules were employed as a linker because its thiol group enables a strong binding with gold and its OH group allows a specific binding with glucose molecules. SERS substrates were immersed into a 1 mM of 4-MPBA solution for 2 h to immobilize the 4-MPBA. Non-immobilized 4-MPBA molecules were removed by rinsing with ethyl alcohol. The SERS substrates were then immersed in various concentrations of glucose solution from 1 to 100 μM. Unbound glucose molecules were eliminated by rinsing the substrates with ethyl alcohol. From the previous results, it was found that the intensity of Raman peaks related with 4-MPBA changed with the injection of glucose and showed a concentration-dependent behavior, which provides an elegant method for the indirect glucose detection [16, 17]. SERS signals of 4-MPBA were measured at five different points and averaged for individual glucose concentrations.

3 Results and discussion

We fabricated three types of SERS substrates by creating GNIs or GNPs on a silicon wafer as shown in the field-emission scanning electron microscope (FE-SEM) images in

Fig. 2. By depositing a 6-nm gold layer using electron beam evaporator, uniform distribution of GNIs was achieved in a large area (see Fig. 2a). GNI thickness of 6 nm was determined as an optimum with the largest SERS peak intensity when the thickness was varied. Also, the CSA technique was applied to attach GNPs on the silicon wafer or the surface of GNIs. While a heterogeneous distribution of aggregated GNPs was obtained in Fig. 2b, the GNPs on the GNI structure were more regularly and densely patterned on the substrate surface (see Fig. 2c). Such a hybrid gold nanostructure with GNIs and GNPs was advantageous for SERS effect due to its nanogap-rich feature. Especially, when the GNPs were located on the gap region of the GNI substrate, we can amplify the local plasmon field significantly and thus lead to a higher SERS signal of the target molecule of interest [18, 19].

The sensitivity and linearity of the three SERS platforms were evaluated by analyzing the Raman intensities for different concentrations of the 4-ABT molecule. In a linear regression analysis, the correlation coefficient (R^2) indicates the degree of linearity and the slope (S) denotes a detection sensitivity. First, for the Sample A, this SERS substrate achieved $R^2 = 0.95$ and $S = 12{,}900$ at 4-ABT concentrations of 10^{-7} to 10^{-3} M at the 1076 cm^{-1} peak, which is assigned to the a_1-type vibrational mode (see Fig. 3a, b). The SERS intensity at the 1-mM concentration was about 35,000 and the average value of the relative standard deviation (RSD), indicating the degree of a signal fluctuation, was obtained to be an excellent value of 7%. We converted the SEM image of Sample A into the binary image to calculate the uniformity of the GNI pattern as shown in Fig. 3c. We analyzed the binary images that consist of black and white pixels over a large area and determined the peak value of gap size distribution of GNIs to be 8 nm in Fig. 3d. The average percentage of gap area was $25.37 \pm 1.41\%$ and its standard deviation values as small as 5% supported a highly uniform distribution of Sample A. Moreover, the finite-element method (FEM) simulation was performed to investigate the characteristic of local plasmon fields when refractive indices (n, k) of silicon and gold at $\lambda = 785$ nm were chosen to be (3.7060, 0.0074) and (0.2313, 4.3933) [20, 21]. Under the assumption that the shape of GNI was a rectangle with a thickness of 6 nm and a gap distance between GNIs of 8 nm, FEM results in Fig. 3e showed that the maximum electric field intensity at the corner of GNIs was 12.3 for an incidence beam of unit amplitude.

Second, for the Sample B, it was found from Fig. 4a, b that the values of correlation coefficient and slope of linear regression were $R^2 = 0.88$ and $S = 26{,}100$, respectively. The SERS intensity at the 4-ABT concentration of 1 mM was about 120,000 and the average RSD was 12%. Sensitivity and SERS intensity larger than the values of Sample A were associated with the aggregation feature of GNPs. Closely aggregated GNPs induced an enhanced nanogap effect, leading to a higher density of hot-spots on the sensor surface. The FEM data of Sample B in Fig. 4c showed a maximum plasmon intensity of 102.1 at the nanogap region, which was amplified by more than an order in comparison with the Sample A. On the other hand, it should be noted that relatively lower R^2 and RSD values can be attributed to non-uniform distribution of GNPs. The heterogeneous spatial distribution of GNPs as shown in Fig. 2b can make it further difficult to perform quantitative analysis [22]. To be specific, the sites which are capable to provide efficient SERS enhancement, were irregularly produced at the total surface area, resulting in strong signal fluctuations.

Third, for the proposed SERS platform with homogeneous GNPs on the GNI pattern, the SERS intensity at the 1076 cm^{-1} peak was increased rapidly up to about 300,000 at the 4-ABT concentration of 1 mM. From the Fig. 4d, e, it is noteworthy that a larger slope of $S = 97{,}900$ and fairly good values of $R^2 = 0.92$ and $RSD = 8\%$ were obtained. This implies that the Sample C has the highest sensitivity among the samples

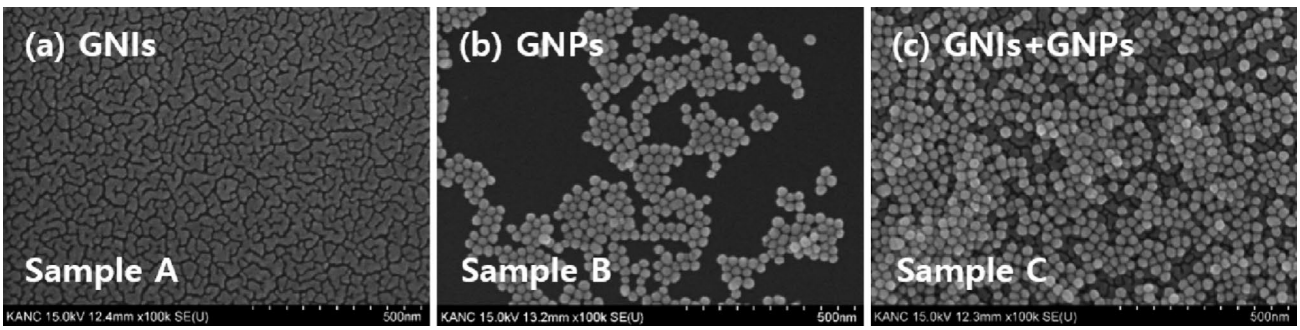

Fig. 2 FE-SEM images of the fabricated SERS substrates with **a** GNIs (Sample A), **b** GNPs (Sample B), and **c** GNPs on the GNI pattern (Sample C). For the Samples A and B, electron beam evaporation and CSA were employed separately to obtain the nanopatterns of GNIs and GNPs

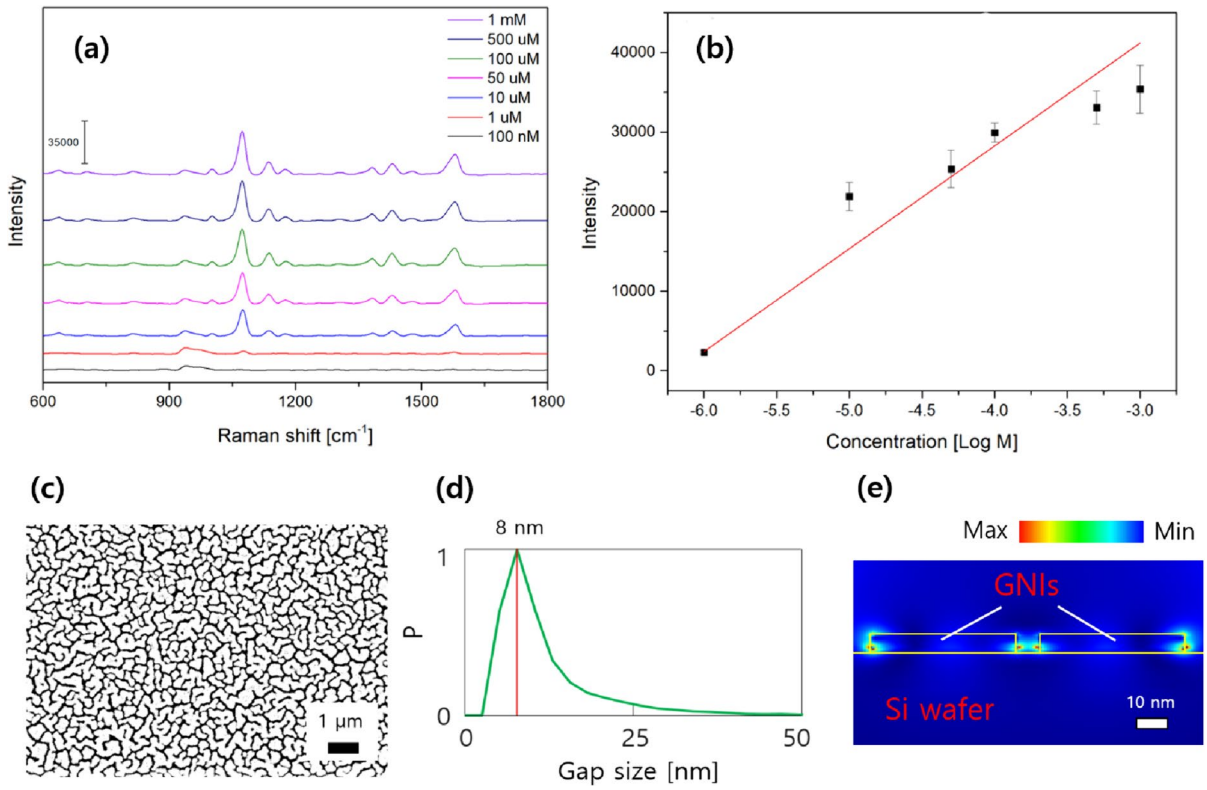

Fig. 3 **a** Raman spectra for a varied concentration of the 4-ABT molecules on the Sample A. **b** Linear regression analysis of the intensity at 1076 cm^{-1} to quantify the sensitivity and linearity. **c** Binary image of the Sample A to calculate its gap size feature. **d** Distribution of the gap size of GNIs for Sample A **e** FEM results for the Sample A when a 785-nm laser light of a unit amplitude has a normal incidence

and allows a reliable detection in a wide range of target concentrations. The largest SERS signal intensity was consistent with the maximum local field intensity of 324.8 in the presence of both GNPs and GNIs, as shown in Fig. 4f. Compared to the FEM results of other samples, the Sample C demonstrated multiple formation of hot-spots between GNPs and at the GNP-GNI gaps and produced an enormous near-field amplification. Further, as the hot-spots were more homogeneously distributed than the Sample B, the fluctuation of SERS signals was notably degraded, leading to an improvement in R^2 and RSD parameters. In short, spatially homogeneous GNPs immobilized on a reliable GNI pattern could be a potential candidate for quantitative SERS detection.

As for the SERS enhancement factor (EF), it was defined as $EF = (I_{SERS}/N_{SERS})/(I_{BULK}/N_{BULK})$, where I_{SERS} and I_{BULK} are the SERS and Raman peak intensities at 1076 cm^{-1} for 4-ABT and N_{SERS} and N_{BULK} are the numbers of 4-ABT molecules on the SERS substrate and 4-ABT powders within a laser spot volume [23]. Raman peak intensities were measured to be $I_{SERS} = 297{,}000$ for Sample C and $I_{BULK} = 10{,}100$. Using the conditions of a laser spot diameter of 10 μm, penetration depth of 20 μm, and 4-ABT molecule size of 0.2 nm^2 [14], the EF was 2.94×10^5 for Sample C, while the values were 3.90×10^4 for Sample A and 2.27×10^5 for Sample B, respectively (Supplementary Information). The SERS EF obtained was consistent with the previous results for nanogap-rich metallic nanostructures [24].

Finally, an application of the proposed SERS platform with GNIs and GNPs was explored by measuring the glucose molecules whose concentration level is used as an indicator of diabetes. Figure 5a shows the schematic of the glucose measurement via a linker of 4-MPBA molecule on the Sample C. When the concentration of 4-MPBA was fixed at 1 mM, the Raman intensity of 4-MPBA at 1067 cm^{-1} has been known to be dependent on the glucose concentration [17, 25]. Such indirect glucose measure was demonstrated in Fig. 5b. In order to estimate the limit of detection (LOD), we defined the blank condition as the case without glucose molecules. By using the blank analysis method, the LOD value is defined as $LOD = m_b + 3s_b$, where m_b and s_b are the mean value and the standard deviation of blank measurements, respectively. When the glucose molecules were not loaded onto 1 mM 4-MPBA, $m_b = 60{,}140$ and $s_b = 10{,}504$ were obtained at the primary peak of 1067 cm^{-1} and thus, the Raman intensity for the LOD was calculated to be 91,652. When the glucose concentration was increased up

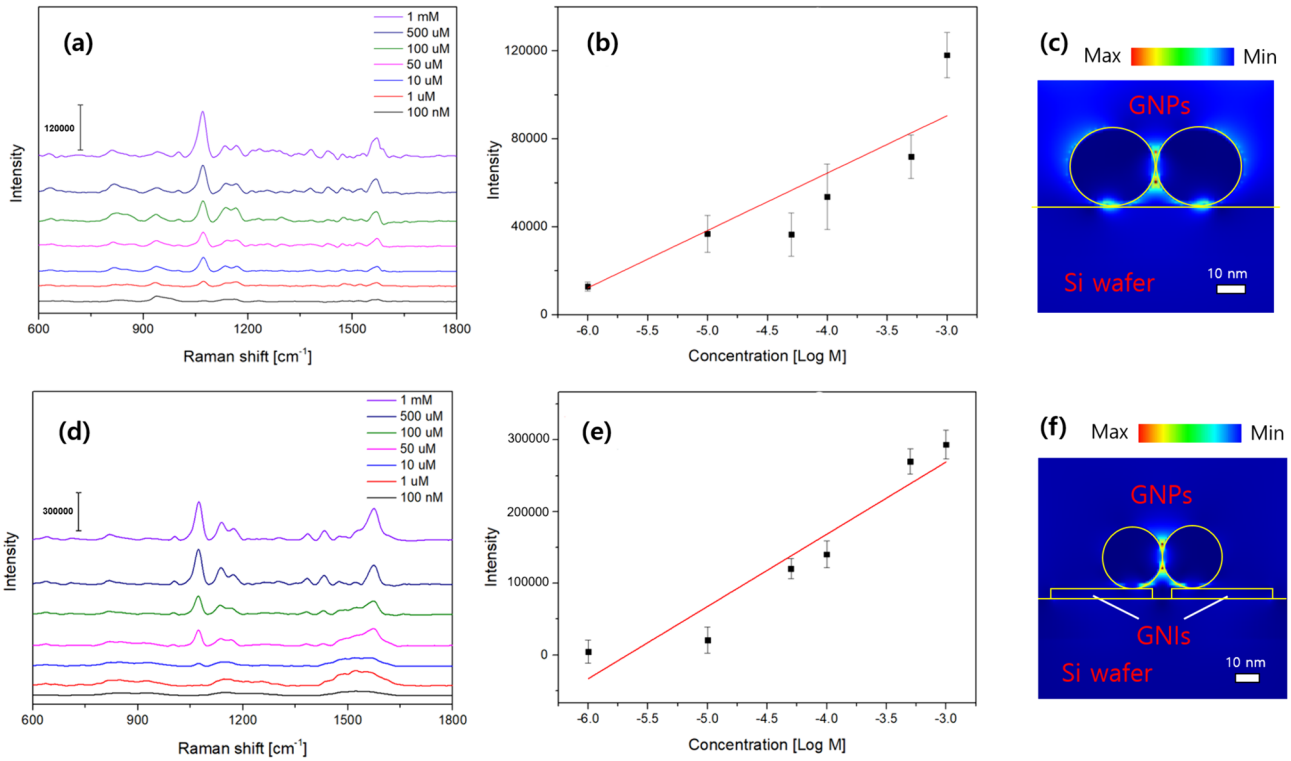

Fig. 4 **a** Raman spectra for a varied concentration of the 4-ABT molecules on the Sample B. **b** Linear regression analysis of the intensity at 1076 cm^{-1}. **c** FEM results for the Sample B. **d** Raman spectra for a varied concentration of the 4-ABT molecules on the Sample C. **e** Linear regression analysis of the intensity at 1076 cm^{-1}**c** FEM results for the Sample C

to 100 µM, the 10 nM concentration with the Raman intensity of 100,711 was determined as the LOD concentration because it exceeded the LOD condition for the first time. From the linear regression analysis in Fig. 5c, the Raman signal showed the highest value of 272,000 at 100 µM and the correlation coefficient was more than 0.90. While the Raman spectra for Sample A were not shown here, in comparison to the Raman intensity of 16,500 for Sample A at 100 µM glucose concentration, Sample C exhibited an enhanced Raman scattering signal by more than 10 times. Further, the 2D Raman mapping was performed at the dimension of 20×20 μm^2 to investigate the spatial reproducibility of the Sample C for glucose monitoring. Figure 5d exhibited the SERS mapping image for the primary peak at the glucose concentration of 100 µM. It was found that the acceptable RSD of 7% was achieved by averaging the Raman intensities for 100 different locations. All these results supported the practicability of the Sample C and the possibility of the accurate and quantitative SERS-based detection of glucose molecules. In our subsequent studies, more reliable and specific binding protocol for a practical glucose sensing will be investigated using real blood samples with various interfering molecules.

4 Conclusion

In summary, we have proposed a synergistic combination of GNPs and GNIs for a sensitive and reliable SERS detection based on two non-lithographic fabrication techniques. Due to a thin gold layer of uniform GNI pattern, immobilization of GNPs via the gold-thiol chemistry was spatially homogeneous compared to the sample with GNPs on a silicon wafer. Since hybrid gold nanostructures with GNPs and GNIs induced multiple and well-distributed hot-spot modes, they contributed to a significantly enhanced Raman intensity and an acceptable reproducibility of Raman signals with a good RSD value of 8%. The FEM computation also supported a high amplification of near-field characteristics in the presence of both GNPs and GNIs. The validity of the suggested strategy was demonstrated by taking glucose molecules as the target analytes. From the indirect glucose measure using a linker of 4-MPBA, high sensitivity more than 10 times, low detection limit as small as 10 nM, and spatially low signal fluctuation less than 7% were achieved. It is thus expected that our novel SERS platform has a great potential for a sensitive and quantitative detection towards a variety of in vitro and in vivo diagnostic applications.

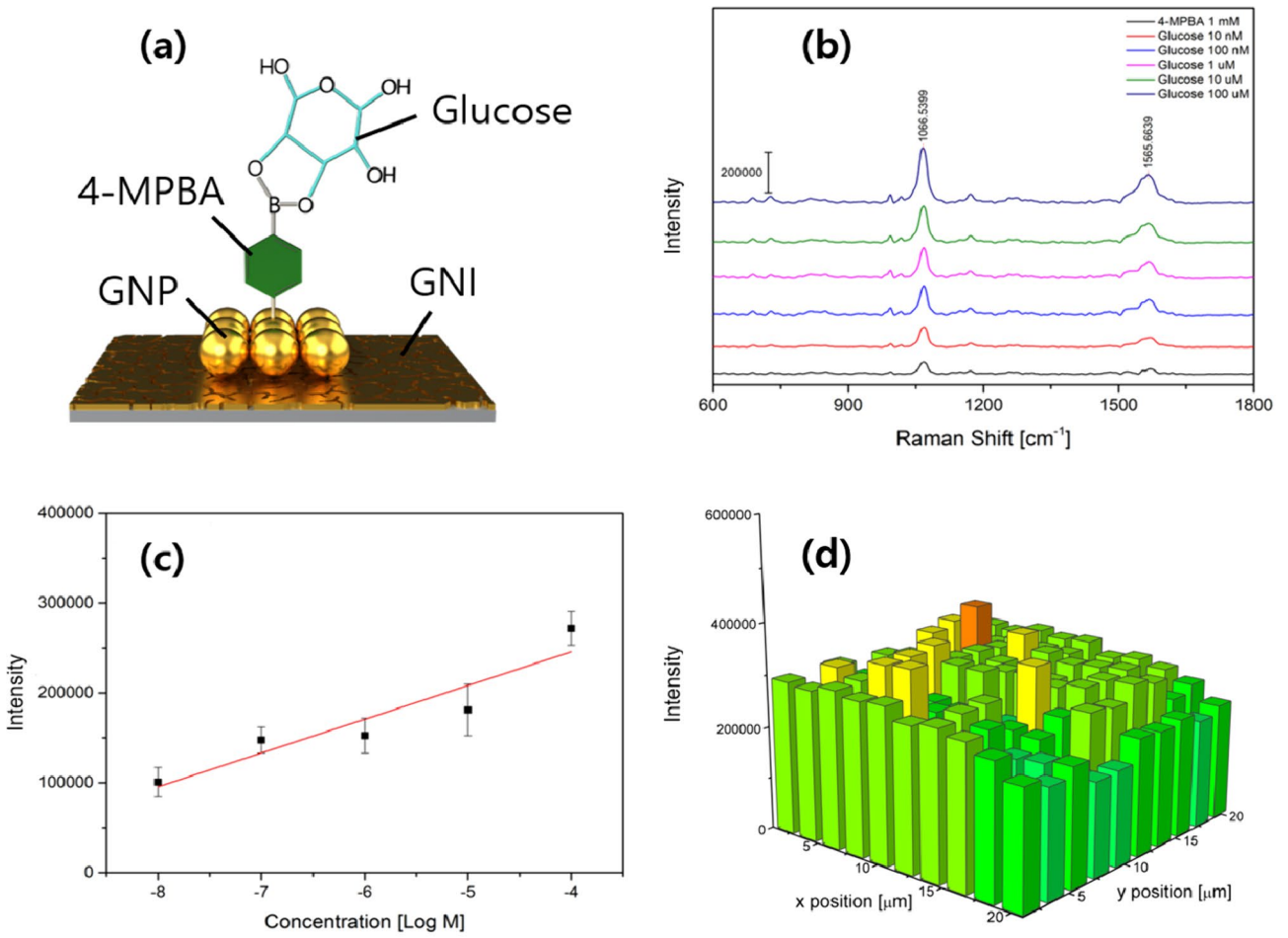

Fig. 5 SERS experiments of glucose molecules. **a** Schematic illustration of chemical binding of glucose via 4-MPBA on the SERS substrate with both GNPs and GNIs. **b** SERS signal profiles of a varied glucose concentration from 0 to 100 μM for a fixed 1-mM 4-MPBA. **c** Linear regression analysis of the intensity at 1067 cm^{-1}. **d** SERS mapping image for the primary SERS peaks at the glucose concentration of 100 μM

Supplementary Information The online version contains supplementary material available at https://doi.org/10.1007/s13534-024-00381-4.

Funding This work was supported by the fund of National Research Foundation of Korea (No. 2022R1A2C1010151, 2022R1C1C1011328, 2022H1D3A2A02081592) and the Brain Korea 21 Four Program. This work was also carried out with the support of "Research Program for Agriculture Science & Technology Development (Project No. RS-2024-00399478)", Rural Development Administration, Republic of Korea.

Declarations

Conflict of interest The authors declare that they have no conflict of interest.

Ethical approval This article does not contain any studies with human participants performed by any of the authors.

References

1. Stiles PL, Dieringer JA, Shah NC, Van Duyne RP. Surface-enhanced Raman spectroscopy. Annu Rev Anal Chem. 2008;1:601–26.
2. Lane LA, Qian X, Nie S. SERS nanoparticles in medicine: from label-free detection to spectroscopic tagging. Chem Rev. 2015;115(19):10489–529.
3. Acharya S, Das B, Thupakula U, Ariga K, Sarma DD, Israelachvili J, Golan Y. A bottom-up approach toward fabrication of ultrathin PbS sheets. Nano Lett. 2013;13(2):409–15.
4. Fu H, Bao H, Zhang H, Zhao Q, Zhou L, Zhu S, Cai W. Quantitative surface-enhanced Raman spectroscopy for field detections based on structurally homogeneous silver-coated silicon nanocone arrays. ACS Omega. 2021;6(29):18928–38.
5. Long L, Ju W, Yang HY, Li Z. Dimensional design for surface-enhanced Raman spectroscopy. ACS Mater Au. 2022;2(5):552–75.
6. Sharma B, Cardinal MF, Kleinman SL, Greeneltch NG, Frontiera RR, Blaber MG, Van Duyne RP. High-performance SERS substrates: advances and challenges. MRS Bull. 2013;38:615–24.

7. De Silva Indrasekara AS. Design criteria to fabricate plasmonic gold nanomaterials for surface-enhanced Raman scattering (SERS)-based biosensing. J Appl Phys. 2021;129:231102.
8. Choi M, Kim S, Choi SH, Park HH, Byun KM. Highly reliable SERS substrate based on plasmonic hybrid coupling between gold nanoislands and periodic nanopillar arrays. Opt Express. 2020;28(3):3598–606.
9. Choi M, Kang T, Choi SH, Byun KM. Dual modal plasmonic substrates based on convective self-assembly technique for enhancement in SERS and LSPR detection. Opt Express. 2021;29(4):6179–87.
10. Xue Y, Li X, Li H, Zhang W. Quantifying thiol–gold interactions towards the efficient strength control. Nat Comm. 2014;5:4348.
11. Watanabe S, Inukai K, Mizuta S, Miyahara MT. Mechanism for stripe pattern formation on hydrophilic surfaces by using convective self-assembly. Langmuir. 2009;25(13):7287–95.
12. Hanafusa T, Mino Y, Watanabe S, Miyahara MT. Controlling self-assembled structure of Au nanoparticles by convective self-assembly with liquid-level manipulation. Adv Pow Technol. 2014;25(2):811–5.
13. Watanabe S, Mino Y, Ichikawa Y, Miyahara MT. Spontaneous formation of cluster array of gold particles by convective self-assembly. Langmuir. 2012;28(36):12982–8.
14. Yoon JK, Kim K, Shin KS. Raman scattering of 4-aminobenzenethiol sandwiched between Au nanoparticles and a macroscopically smooth Au substrate: Effect of size of Au nanoparticles. J Phys Chem C. 2009;113(5):1769–74.
15. Zhu J, Wu N, Zhang F, Li X, Li J, Zhao J. SERS detection of 4-Aminobenzenethiol based on triangular Au–AuAg hierarchical-multishell nanostructure. Spectrochim Acta A. 2018;204:754–62.
16. Sun X, Stagon S, Huang H, Chen J, Lei Y. Functionalized aligned silver nanorod arrays for glucose sensing through surface enhanced Raman scattering. RSC Adv. 2014;4(45):23382–8.
17. Yang D, Afroosheh S, Lee JO, Cho H, Kumar S, Siddique RH, Choo H. Glucose sensing using surface-enhanced Raman-mode constraining. Anal Chem. 2018;90(24):14269–78.
18. Nam JM, Oh JW, Lee H, Suh YD. Plasmonic nanogap-enhanced Raman scattering with nanoparticles. Acc Chem Res. 2016;49(12):2746–55.
19. Liang Y, Li L, Lu M, Yuan H, Long Z, Peng W, Xu T. Comparative investigation of sensing behaviors between gap and lattice plasmon modes in a metallic nanoring array. Nanoscale. 2018;10(2):548–55.
20. Aspnes DE, Studna AA. Dielectric functions and optical parameters of Si, Ge, GaP, GaAs, GaSb, InP, InAs, and InSb from 1.5–6.0 eV. Phys Rev B. 1983;27(2):985–1009.
21. Rakić AD, Djurišić AB, Elazar JM, Majewski ML. Optical properties of metallic films for vertical-cavity optoelectronic devices. Appl Opt. 1998;37(22):5271–83.
22. Norton RD, Phan HT, Gibbons SN, Haes AJ. Quantitative surface-enhanced spectroscopy. Annu Rev Phys Chem. 2022;73:141–62.
23. Lovera P, Creedon N, Alatawi H, Mitchell M, Burke M, Quinn AJ, O'Riordan A. Low-cost silver capped polystyrene nanotube arrays as super-hydrophobic substrates for SERS applications. Nanotechnol. 2014;25(17): 175502.
24. Litti L, Meneghetti M. Predictions on the SERS enhancement factor of gold nanosphere aggregate samples. Phys Chem Chem Phys. 2019;21(28):15515–22.
25. Choi SE, Park D, Hwang H, Seo M, Lee D, Jeong U, Kim JW. 2D colloidal array of glucose-conjugative conductive microparticles for a pressure-mediated chemiresistive sensor platform. Adv Funct Mater. 2020;30:2000431.